



Journal of Applied and Computational Mechanics



Research Paper

Hydrodynamic Behavior in Solar Oil Heat Exchanger Ducts Fitted with Staggered Baffles and Fins

Younes Menni¹, Ali J. Chamkha², Houari Ameer³, Mohammad Hossein Ahmadi⁴

¹ Unit of Research on Materials and Renewable Energies, Department of Physics, Faculty of Sciences, Abou Bekr Belkaid University BP 119-13000-Tlemcen, Algeria, Email: menniyounes.cfd@gmail.com

² Faculty of Engineering, Kuwait College of Science and Technology, Doha, Kuwait, Email: a.chamkha@kcst.edu.kw

³ Department of Technology, University Centre of Naama, P.O. Box 66, Naama 45000, Algeria, E-mail: houari_ameur@yahoo.fr

⁴ Faculty of Mechanical Engineering, Shahrood University of Technology, Shahrood, Iran, E-mail: mohammadhosein.ahmadi@gmail.com

Received January 31 2020; Revised March 30 2020; Accepted for publication April 26 2020.

Corresponding author: Y. Menni (menniyounes.cfd@gmail.com)

© 2022 Published by Shahid Chamran University of Ahvaz

Abstract. The attachment of turbulators, such as baffles, fins, ribs, bars, and blocks, inside the thermal solar receiver ducts, is among the most effective mechanisms for important thermal exchange by creating the turbulence, extending the trajectory of the flow, increasing the surface of heat exchange, forcing recycling cells, and hence a high thermal exchange. The solar finned and baffled heat exchangers are employed in a wide application interval, and it is important to examine the design of a duct for this configuration of the flow field and its effect on the heat transport phenomenon. In This study, dynamic field simulations are reported in horizontal rectangular form ducts, using three obstacles with oil HTF (heat transfer fluid). Two various finned and baffled duct configurations are treated, i.e., case (A) with one fin and two baffles, and case (B) with two fins and one baffle. Different hydrodynamic fields, i.e., X-velocity and Y-speed, as well as various X-velocity profiles in many flow stations, related to Re value, are analyzed. A computational approach is applied in order to simulate the oil flow, using finite volume (FV) integration method, SIMPLE discretization algorithm, QUICK interpolation scheme, Standard k -epsilon turbulence model, and ANSYS FLUENT 12.0 software. Simulation results reported an unstable flow structure, with powerful recycling cells, on the backsides of each fin and baffle, as a result of fluid detachment at their upper front sharp edges, in both studied models (A and B). As expected, the first duct model, i.e., Case A, has better X- and Y-velocity values, due to its large recirculation regions. In This paper, many physical phenomena, such as the turbulence, instability, flow separation, and the appearance of reverse secondary currents, are reported. As its data confirmed by many previous numerical and experimental results, the suggested new models of finned and baffled heat exchangers filled with high thermal conductivity oil, allow an improvement in the dynamic thermal-energy behavior of many thermal devices such as flat plate solar collectors.

Keywords: Solar finned and baffled heat exchangers, flat plate solar collectors, dynamic thermal-energy behavior, CFD.

1. Introduction

It is well known that the energy output of any solar baffled and finned heat exchanger is mainly related to a set of factors, such as the duct geometry, baffle and fin dimensions and shapes, boundary conditions, pure or composite fluid nature, physical data of the fluid, etc. These factors greatly affect the flow field and change the hydrodynamic characteristics, which affect the heat transfer between the hot zones and working fluid (for example, see Berner et al. [1], Habib et al. [2], Yuan et al. [3], Cheng and Huang [4], Hong and Hsieh [5], Bazdidi-Tehrani and Naderi-Abadi [6], Demartini et al. [7], Li and Kottke [8], Mousavi and Hooman [9], Pirouz et al. [10], Mokhtari et al. [11], Webb and Ramadhyani [12], Wen et al. [13], Dong et al. [14], Skullong et al. [15], Thianpong et al. [16], Nanan et al. [17], Promvong [18], Eiamsa-ard et al. [19], Chamoli [20], and Kumar et al. [21]). The majority of these research projects relied mainly on the technique of reconfiguring the internal geometry of the ducts and channels by introducing new baffles and fins of very complex geometric irregular shapes; see Tables 1 and 2. Other researchers have used various nanofluids, porous medias, perforated turbulators, solid deflectors, and vortex generators to favor the heat and mass transfer (for example, see Oguntala et al. [22], Davies [23], Sobamowo and Kamiyo [24], Caccia et al. [25], Ghahremani et al. [26], Amy et al. [27], Akinshilo et al. [28], Tolstoy et al. [29], Oguntala and Abd-Alhameed [30], and Amari et al. [31]).

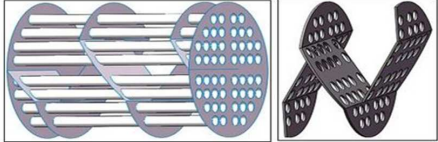
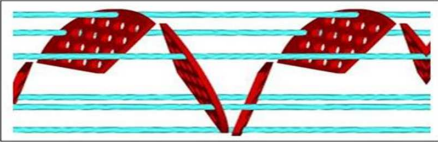
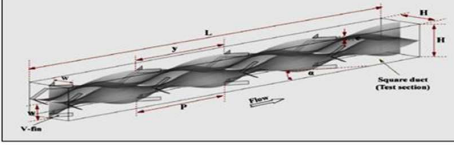
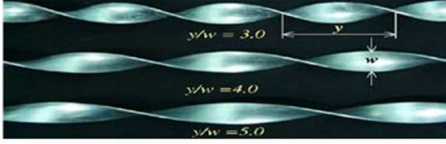
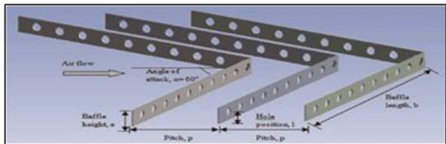
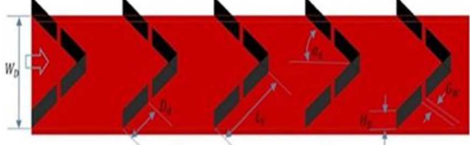


Table 1. Numerical and experimental baffled channels.

Authors	Study/flow regime	Geometry
Berner et al. (1984)	Experimental study Turbulent and laminar flow	<p>Flow around baffles [1]</p>
Habib et al. (1988)	Computational analysis Turbulent flow	<p>Channel with streamwise-periodic flow [2]</p>
Yuan et al. (1998)	Numerical prediction Laminar flow	<p>Channel with streamwise-periodic rod disturbances [3]</p>
Cheng and Huang (1991)	Numerical prediction Laminar flow	<p>Parallel-plate channels with transverse fin arrays [4]</p>
Hong and Hsieh (1991)	Experimental investigation turbulent flow	<p>Square duct with staggered ribs [5]</p>
Bazdidi-Tehrani and Naderi-Abadi (2004)	Numerical analysis Laminar flow	<p>Horizontal channel with transverse fins [6]</p>
Demartini et al. (2004)	Numeric and experimental analysis Turbulent flow	<p>Channel with baffle plates [7]</p>
Li and Kottke (1998)	Experimental study Turbulent and laminar flows	<p>Staggered tube arrangement [8]</p>
Mousavi and Hooman (2006)	Numerical investigation Laminar flow	<p>Channel with staggered baffles [9]</p>
Pirouz et al. (2011)	Numerical simulation Laminar flow	<p>Rectangular channel with wall-mounted obstacles [10]</p>
Mokhtari et al. (2017)	Numerical study Turbulent and laminar flows	<p>Fin arrangements in a horizontal channel [11]</p>
Webb and Ramadhyani (1985)	Numerical simulation Laminar flow	<p>Channel with staggered ribs [12]</p>



Table 2. Baffle and fin reconfiguration.

Investigators	Study/flow regime	Configuration
Wen et al. (2015)	Experimental investigation Turbulent flow	 <p>Shell-and-tube heat exchangers with different baffles [13]</p>
Dong et al. (2017)	Numerical investigation Turbulent flow	 <p>Trisection helical baffles heat exchangers [14]</p>
Skullong et al. (2016)	Experimental and numerical study Turbulent flow	 <p>Channel with oblique horseshoe baffles [15]</p>
Thianpong et al. (2012)	Experimental investigation Turbulent flow	 <p>Heat exchangers fitted with twisted-ring turbulators [16]</p>
Nanan et al. (2016)	Experimental and numerical study Turbulent flow	 <p>Heat exchanger tube with twisted cross-baffle turbulators [17]</p>
Promvong (2015)	Experimental investigation Turbulent flow	 <p>Heat exchanger with quadruple V-finned twisted tapes [18]</p>
Eiamsa-ard et al. (2010)	Experimental investigation Turbulent flow	 <p>Tube with delta-winglet twisted tape inserts [19]</p>
Chamoli (2015)	Experimental study Turbulent flow	 <p>Channel roughened with V-down perforated baffles [20]</p>
Kumar et al. (2016)	Experimental analysis Turbulent flow	 <p>Channel with broken multiple V-type baffle [21]</p>



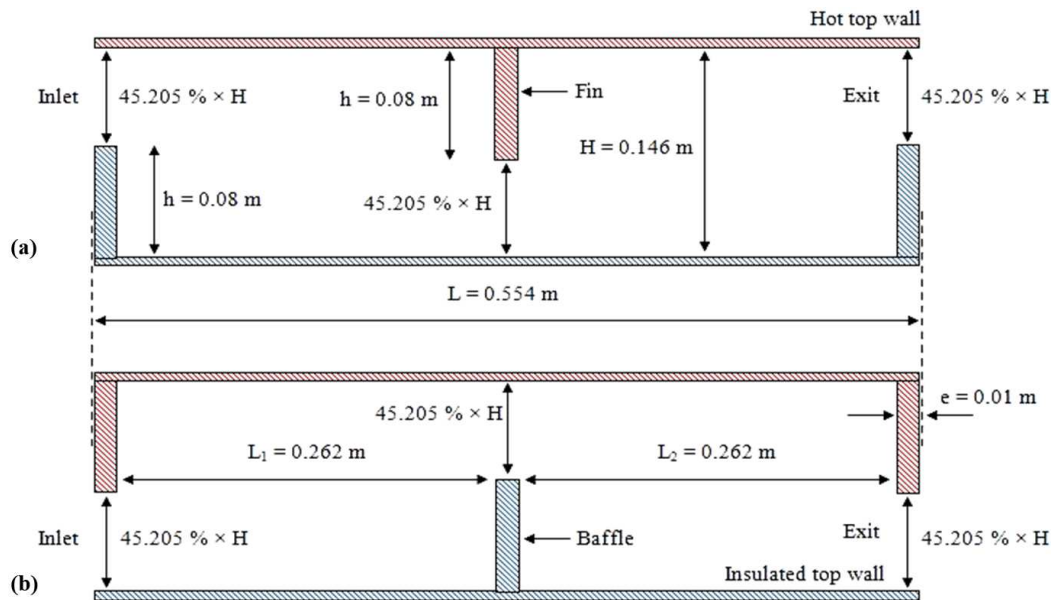


Fig. 1. Pipe models used: (a) A model, (b) B model [32].

Solar duct heat exchangers are heat transfer devices that convert the solar radiation into heat energy for use in various fields. Due to the increasing demand on the use of the thermal energy, it has become necessary to search for advanced thermal receptors with high energy efficiency by improving their dynamic and thermal characteristics. Many researchers, as we mentioned earlier at the top, have focused their studies on how to improve the fluid flow inside the ducts contained in these solar receptors, such as adding extended areas as fins and baffles.

In most of these scientific attempts, the only heat transfer fluid used is air. Whereas, this fluid is weak, in terms of thermo-physical properties, such as the density and thermal conductivity. For this, the energetic efficiency yield of these thermal receptors was very low. This is what prompted us to search for a new fluid with elevated thermo-physical properties, which would enable it to acquire a greater amount of heat energy as it comes into contact with the hot spaces of the duct.

In this scope, our study adopted a combination of two methods. The first method involved changing the vein of the fluid by inserting transverse obstacles in order to create gaps, secreting recycling cells and allowing the fluid to acquire significant heat energy. The second method involved compensating the air with a high thermal conductivity Oil fluid in order to increase the heat transfer between the two media. Both methods help dynamically and thermally improve the energetic performance. Through this study, we will study the dynamic behavior of the adopted Oil fluid by analyzing and discussing flow fields in terms of velocity, as well as examining axial velocity curves at different locations of the duct to reveal the hydrodynamic characteristics of each duct region. The results of this simulation will serve as a database for studying the thermal performance of these solar receptors in the future researches.

2. Mathematical Foundation

2.1 Flow Geometry

Enhancement of flow characteristics of oil fluid in horizontal ducts by installing flat rectangular baffles and fins is addressed in Fig. 1. The baffled duct design and its impact on the turbulence phenomenon are studied, using a CFD (Computational Fluid Dynamics) technique. Two different duct configurations are considered through this analysis. In the first situation, as in Fig. 1a, a first duct with one fin and two baffles is studied (Case A), and in the second proposition, as in Fig. 1b, a second duct with two fins and one baffle is investigated (Case B). All concerned geometry dimensions and considered boundary conditions are also presented in Fig. 1. This study is complementary to the study mentioned in the referenced paper [32].

2.2 Physical Model

Several simplifications were taken in this study, as follows:

- Oil HTF is steady.
- Oil HTF is turbulent.
- Oil HTF is incompressible.
- Oil HTF density ρ_f is constant.
- Oil HTF specific heat C_p is constant.
- Oil HTF dynamic viscosity μ_f is constant.
- Oil HTF thermal conductivity k_f is constant.

The ρ_f , C_p , μ_f , and k_f properties are found in [33].

2.3 Boundary Conditions

The various boundary conditions used are as follows:

- Oil HTF velocity for $x = 0$, is $u = U_{in}$ [7,34]
- Oil HTF temperature for $x = 0$, is $T_{in} = 298$ K [33],
- Oil HTF pressure for $x = L$, is $P = P_{atm}$ [7],
- Temperature of the wall with $y = H/2$ is $T_w = 375$ k [34], and
- Wall with $y = -H/2$ is insulated.



2.4 Governing Equations

The mathematical relationship describing the fluid flow within the considered baffled and finned ducts can be written as follows:

$$\frac{\partial}{\partial x}(\rho u \varphi) + \frac{\partial}{\partial y}(\rho v \varphi) = \frac{\partial}{\partial x} \left[\Gamma_{\varphi} \frac{\partial \varphi}{\partial x} \right] + \frac{\partial}{\partial y} \left[\Gamma_{\varphi} \frac{\partial \varphi}{\partial y} \right] + S_{\varphi} \quad (1)$$

with

$\phi \equiv (u, v, k, \varepsilon \text{ and } T)$,

u : x-velocity,

v : y-velocity,

k : turbulent kinetic energy,

ε : turbulent dissipation rate,

Γ_{ϕ} : turbulent diffusion coefficient, and

S_{ϕ} : source term.

Equations for ϕ , Γ_{ϕ} and S_{ϕ} :

Continuity:

$$\varphi = 1 \quad (2)$$

$$\Gamma_{\varphi} = 0 \quad (3)$$

$$S_{\varphi} = 0 \quad (4)$$

X-momentum:

$$\varphi = u \quad (5)$$

$$\Gamma_{\varphi} = \mu_e \quad (6)$$

$$S_{\varphi} = \frac{\partial P}{\partial x} + \frac{\partial}{\partial x} \left[\mu_e \left(\frac{\partial u}{\partial x} \right) \right] + \frac{\partial}{\partial y} \left[\mu_e \left(\frac{\partial v}{\partial x} \right) \right] \quad (7)$$

Y-momentum:

$$\varphi = v \quad (8)$$

$$\Gamma_{\varphi} = \mu_e \quad (9)$$

$$S_{\varphi} = \frac{\partial P}{\partial y} + \frac{\partial}{\partial x} \left[\mu_e \left(\frac{\partial u}{\partial y} \right) \right] + \frac{\partial}{\partial y} \left[\mu_e \left(\frac{\partial v}{\partial y} \right) \right] \quad (10)$$

Fluid energy:

$$\varphi = T \quad (11)$$

$$\Gamma_{\varphi} = \frac{\mu_e}{\sigma_T} \quad (12)$$

$$S_{\varphi} = 0 \quad (13)$$

At solid Energy:

$$\varphi = T \quad (14)$$

$$\Gamma_{\varphi} = k_s \quad (15)$$

$$S_{\varphi} = \frac{\partial}{\partial x}(\rho_s u T) + \frac{\partial}{\partial y}(\rho_s v T) \quad (16)$$

Turb-Kinetic-energy (k):

$$\varphi = k \quad (17)$$



$$\Gamma_{\varphi} = \mu_l + \frac{\mu_t}{\sigma_k} \quad (18)$$

$$S_{\varphi} = -\rho\varepsilon + G_k \quad (19)$$

Turbulence dissipation rate (ε):

$$\varphi = \varepsilon \quad (20)$$

$$\Gamma_{\varphi} = \mu_l + \frac{\mu_t}{\sigma_{\varepsilon}} \quad (21)$$

$$S_{\varphi} = \frac{\varepsilon}{k} (C_{1\varepsilon} G_k - C_{2\varepsilon} \rho\varepsilon) \quad (22)$$

with

$$\mu_{\text{eff}} = \mu_l + \mu_t \quad (23)$$

$$\mu_t = f_{\mu} \rho C_{\mu} \frac{k^2}{\varepsilon} \quad (24)$$

$$G_k = \mu_t \left\{ 2 \left[\left(\frac{\partial u}{\partial x} \right)^2 + \left(\frac{\partial v}{\partial y} \right)^2 \right] + \left(\frac{\partial u}{\partial y} + \frac{\partial v}{\partial x} \right)^2 \right\} \quad (24)$$

and

$$C_{1\varepsilon} = C_{3\varepsilon} = 1.44, C_{2\varepsilon} = 1.92, C_{\mu} = 0.09, \sigma_k = 1.0, \sigma_{\varepsilon} = 1.3, \text{ and } \sigma_T = 0.85 \quad (26)$$

2.5 Governing Parameters

Reynolds number (Re):

$$\text{Re} = \rho \bar{U} D_h / \mu \quad (27)$$

Hydraulic diameter (D_h):

$$D_h = 2HW / (H + W) \quad (28)$$

Petukhov correlation [35]:

$$f_0 = (0.79 \ln \text{Re} - 1.64)^{-2} \quad (29)$$

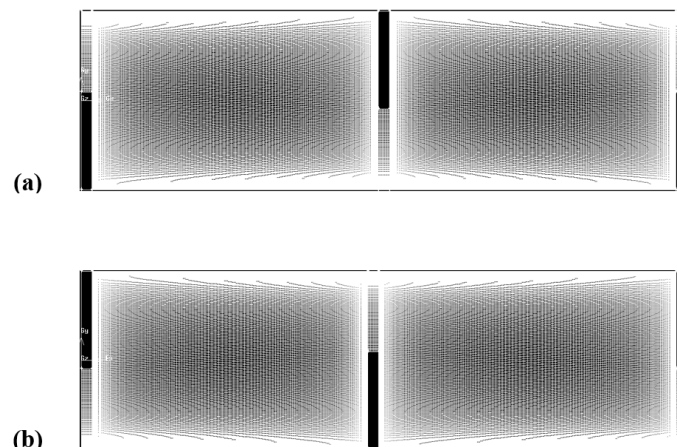


Fig. 2. Computational domain mesh: (a) case A, and (b) case B.



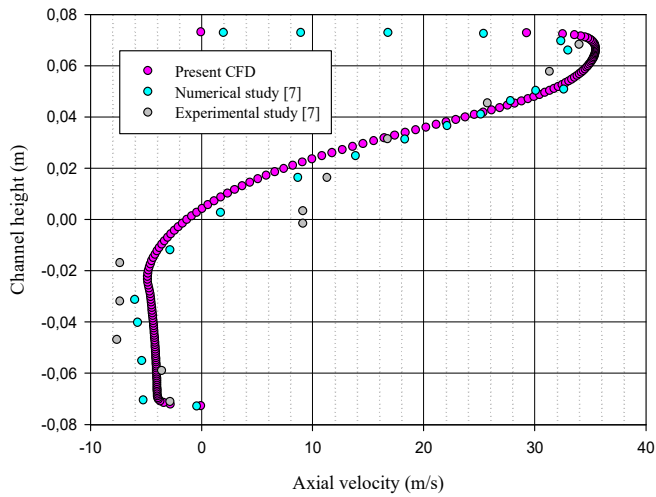


Fig. 3. Validation of the present profiles of X-velocity with the referenced data (Demartini et al., 2004) at $x = 0.525$ m, under similar geometry and fluid flow conditions (a rectangular channel with staggered two baffle plates, turbulent air flow, and $U_{in} = 7.8$ m/s).

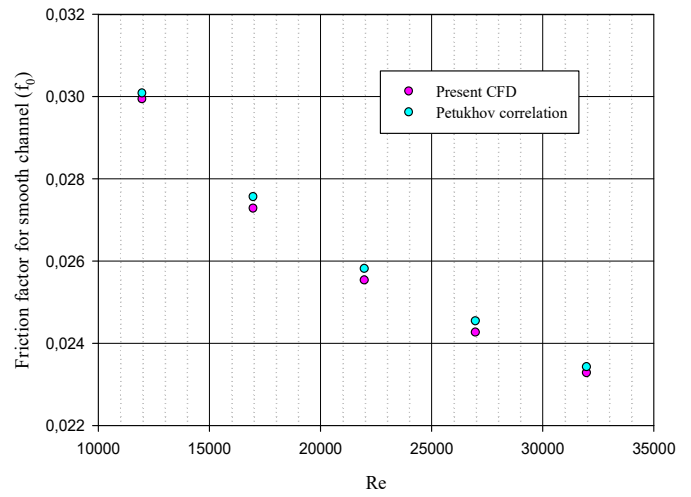


Fig. 4. Verification of the friction factor (f_0) for the present smooth channel with the referenced empirical correlation [35].

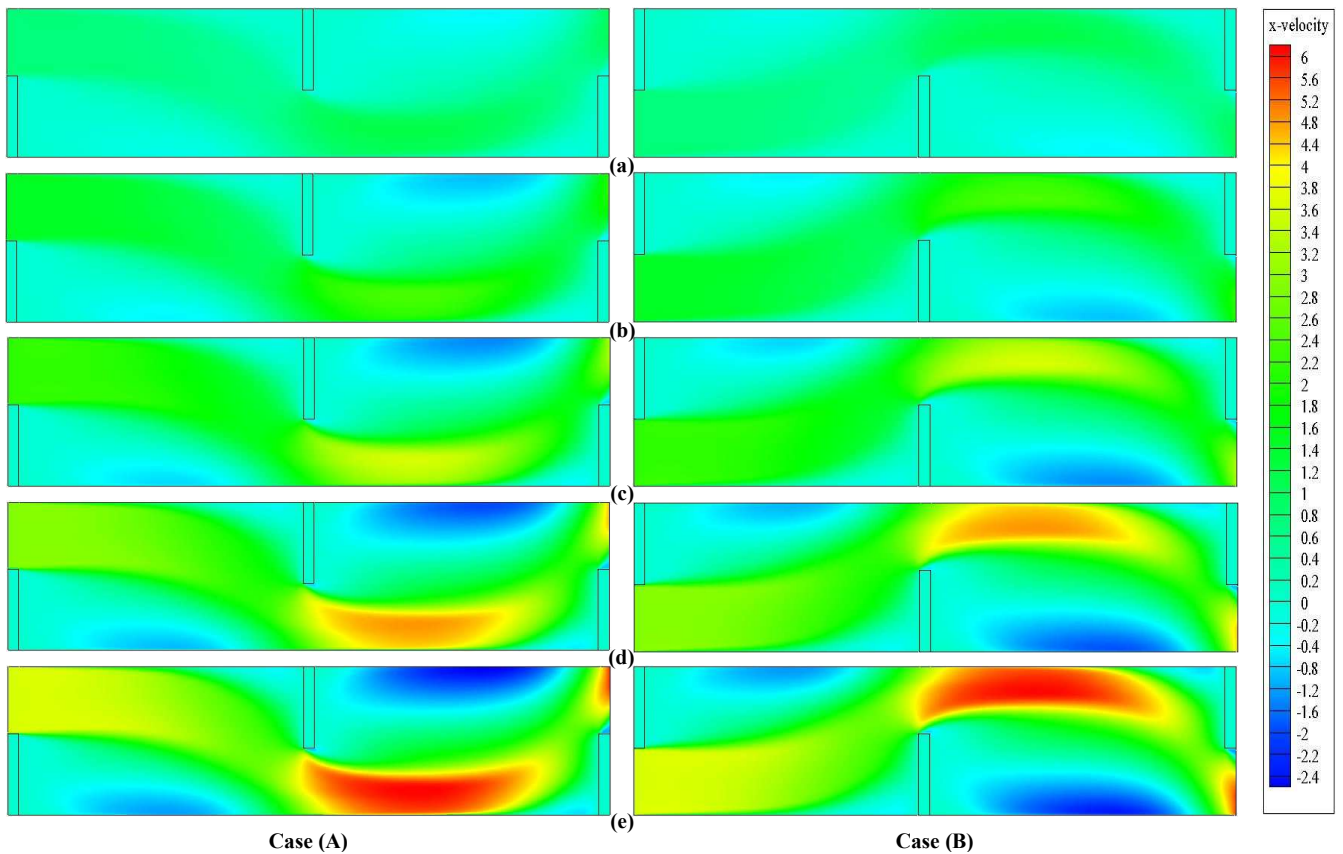


Fig. 5. Contours of X-velocity in A and B cases: $Re = (a) 5 \times 10^3, (b) 10^4, (c) 1.5 \times 10^4, (d) 2 \times 10^4, \text{ and } (e) 2.5 \times 10^4$.

3. Numerical Model

3.1 Numerical Methods

The system of Eq. (1) is solved numerically using the following:

- Standard k -epsilon (k - ϵ) turbulence model [36],
- Finite Volume (VF) method [37],
- SIMPLE discretization formulation [37],
- QUICK interpolation scheme [38], and
- ANSYS FLUENT simulation software [39].



3.2 Numerical Mesh

In this study, a two-dimensional mesh is used according to the horizontal (X) and vertical (Y) axes, with quadrilateral shaped cells. It is an irregular grid near the solid limits of the duct walls as well as the sides of the fins and baffles. Whereas, this mesh is regular far from these solid boundaries; Fig. 2 gives the model of the mesh used.

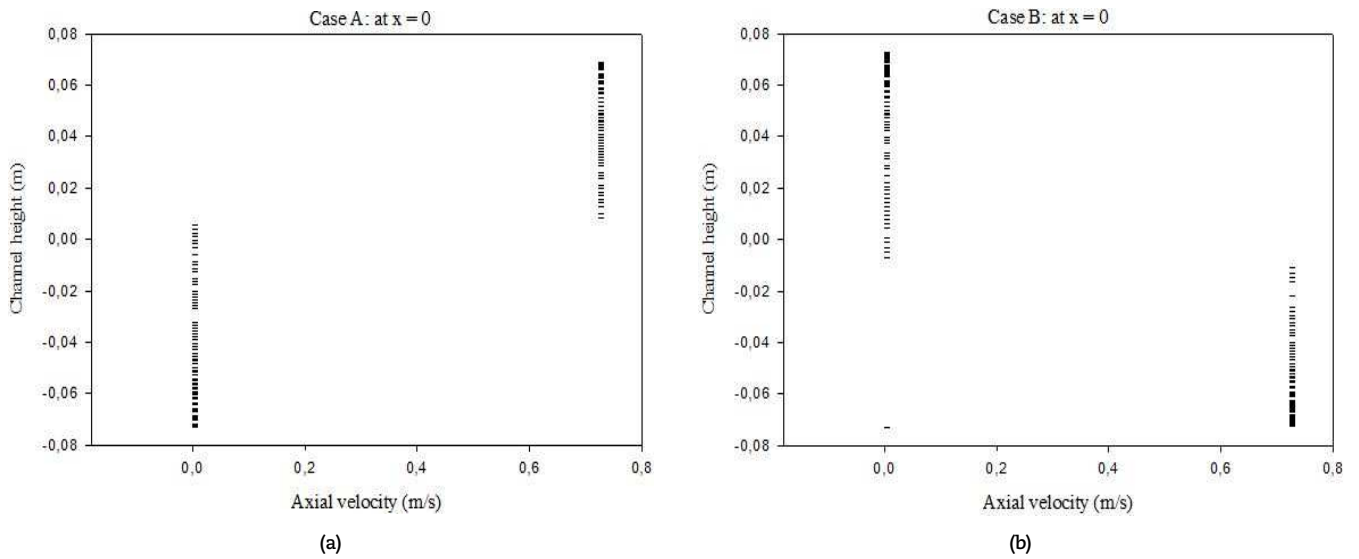


Fig. 6. u at $x = 0$ in (a) A, (b) B case, $Re = 5,000$.

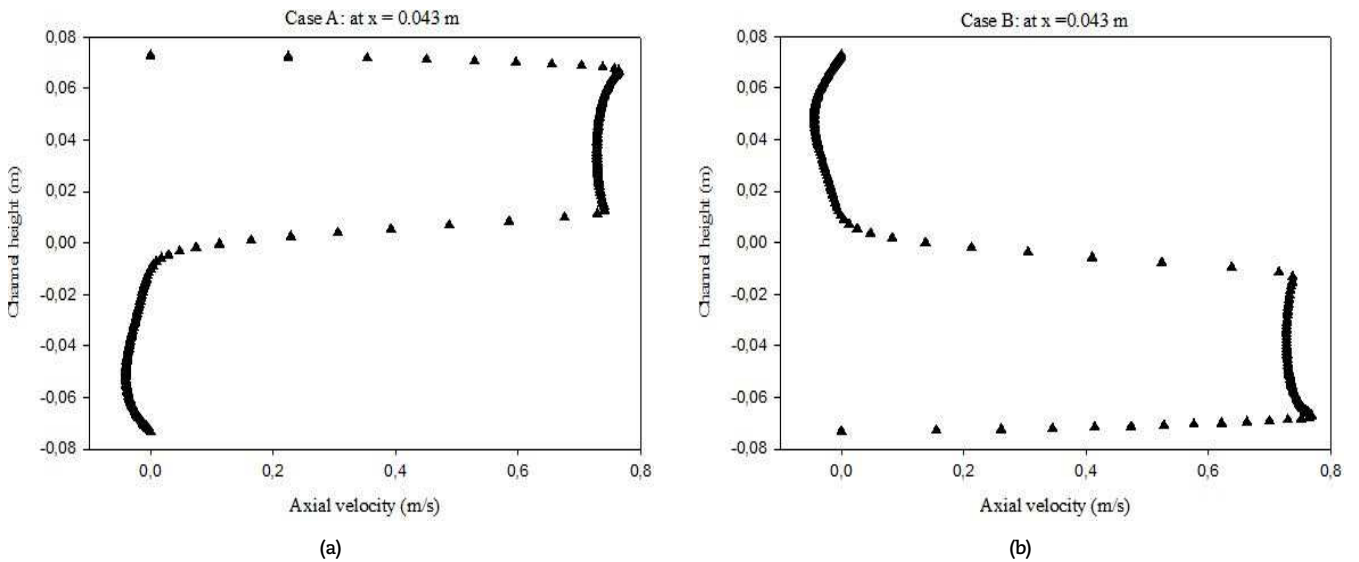


Fig. 7. u at $x = 0.043$ m in (a) A, (b) B case, $Re = 5,000$.

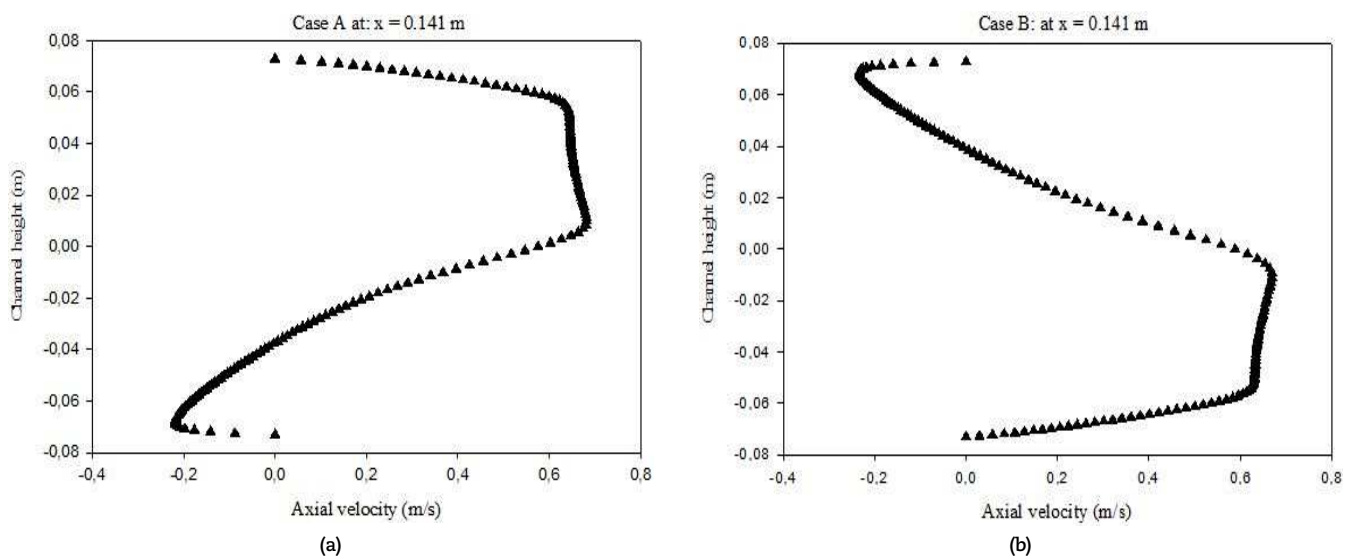


Fig. 8. u at $x = 0.141$ m in (a) A, (b) B case, $Re = 5,000$.



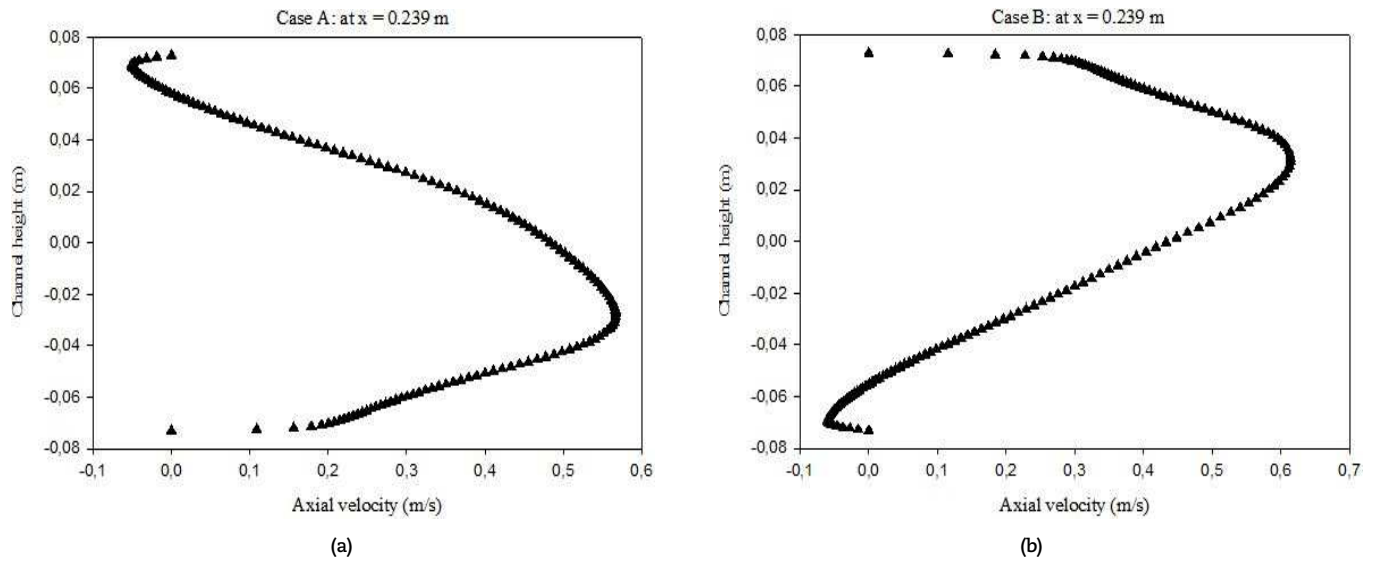


Fig. 9. u at $x = 0.239$ m in (a) A, (b) B case, $Re = 5,000$.

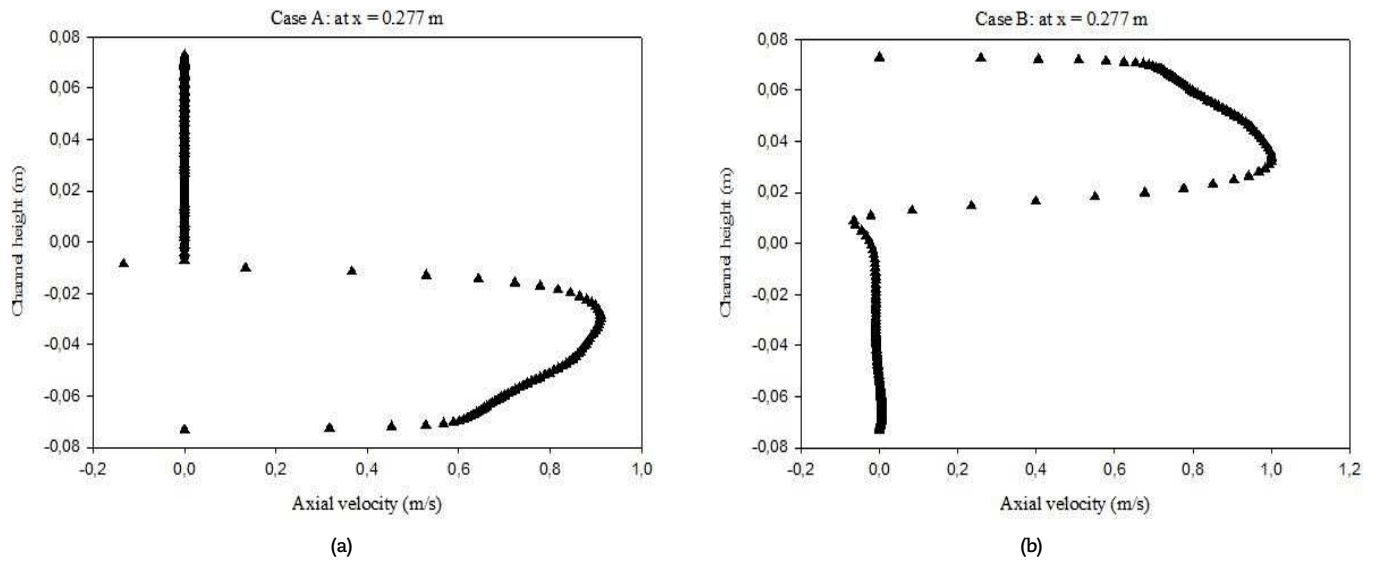


Fig. 10. u at $x = 0.277$ m in (a) A, (b) B case, $Re = 5,000$.

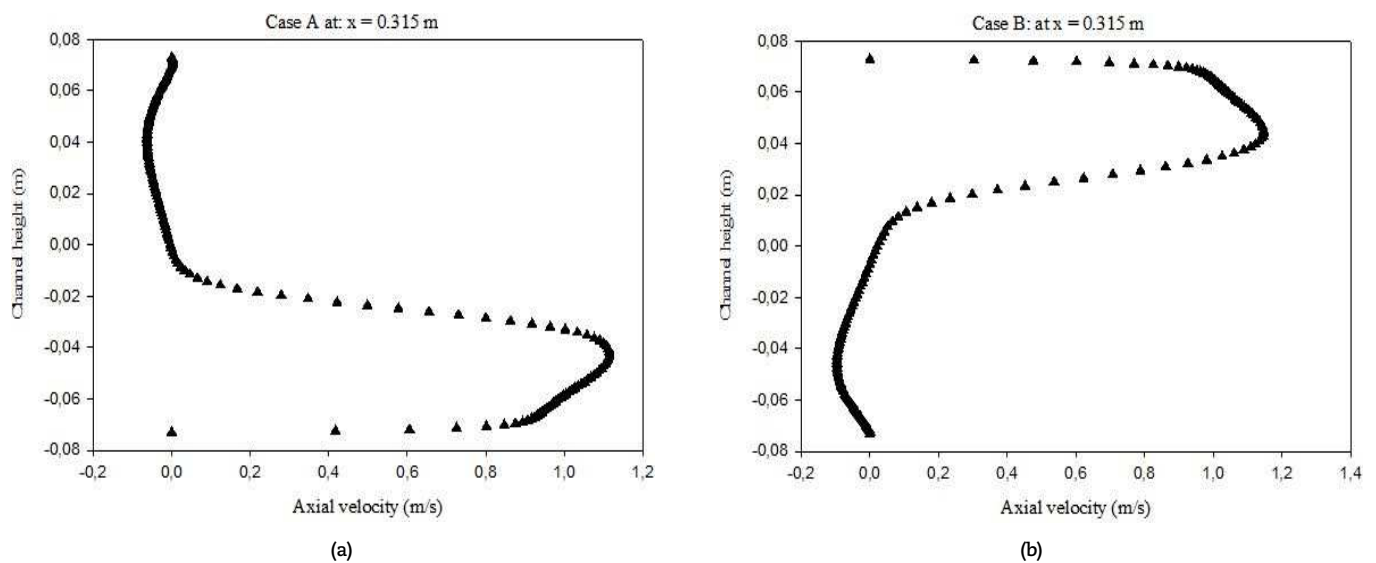


Fig. 11. u at $x = 0.315$ m in (a) A, (b) B case, $Re = 5,000$.

Several node densities ($N_x \times N_y$) were verified in order to obtain a mesh independent of the numerical solution, by comparing various grids, i.e. (95×35) , (120×45) , (145×55) , (170×65) , (195×75) , (220×85) , (245×95) , and (370×145) cells. The comparison stated that the grid of (245×95) cells is considered to be an optimal mesh system by comparing it with the reference pair of (370×145) cells. So, the grid system of (245×95) cells is used during the simulation length of this study.



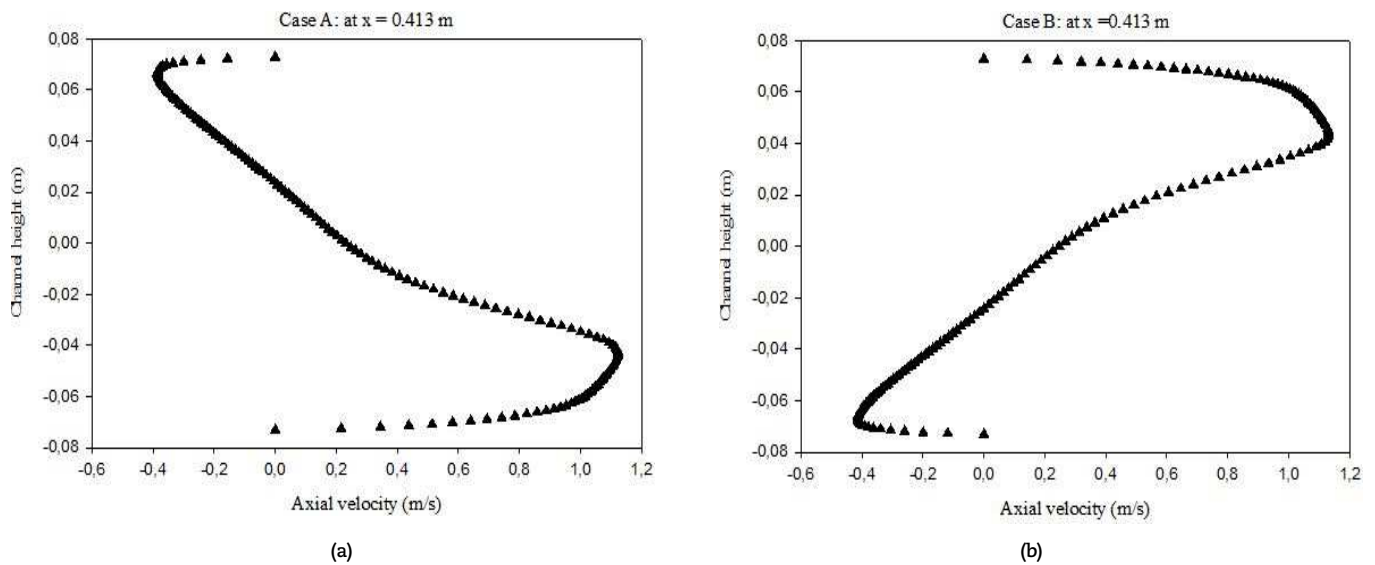


Fig. 12. u at $x = 0.413$ m in (a) A, (b) B case, $Re = 5,000$.

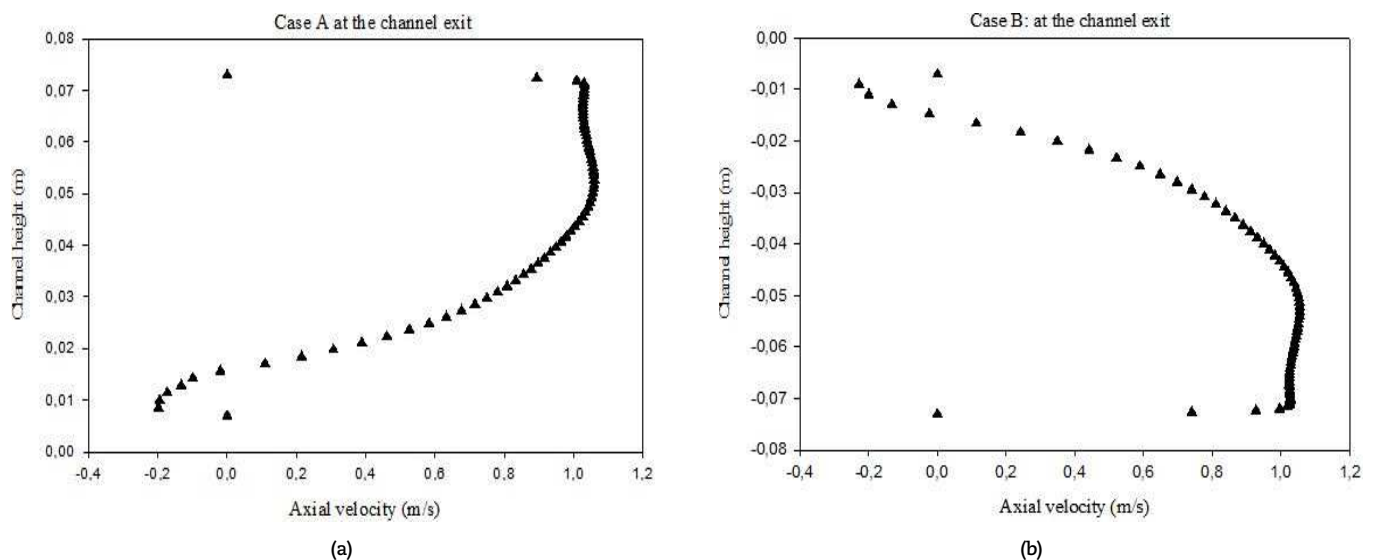


Fig. 13. u at $x = 0.554$ m in (a) A, (b) B case, $Re = 5,000$.

3.3 Numerical Validation with Referenced Numerical and Experimental Data

Fig. 3 reports a comparison of axial velocity (u) values obtained in the present simulation with that of the numerical and experimental values provided by Demartini et al. [7]. This comparison was made by relying on the same flow and geometry conditions reported by the referenced paper [7], which gave the same behavior both quantitatively and qualitatively, and this indicates the validity of the numerical model that is used in this research work.

3.4 Numerical Verification with Smooth Channels

In addition, there is a preview of the pressure drop values in terms of friction factor (f_o) in the case of the smooth channel by relying on the empirical correlation of Petukhov [35] as shown in Fig. 4. The plot shows a good agreement between the simulation and correlation data.

4. Results and Discussion

This type of analysis is very useful in many industry and engineering related problem for getting good idea about the physical model whenever the analytic solution is out of reach. The axial velocity (X -velocity or u) fields are presented in this study for a good analysis of the effect of the staggered obstacles and the nature of the fluid along with the internal structure of the duct on the dynamics of the flow field in both cases investigated (A and B), as reported in Fig. 5a-e.

As shown in Fig. 5a-e,

- Values of u are very high near the duct walls, between the last two obstacles, as well as near their upper frontal sides. This rise in the axial velocity is the result of a change in the stream direction due to the turbulators, as reported numerically in [12], for staggered rib and fin type obstacles in parallel plate type ducts.
- Values of u are also increased between the turbulator sharp edges and the duct wall surfaces due to the higher dynamic pressure values caused by the reduction in the stream surface. Similar behavior was found numerically and experimentally in [1, 4-7, 10].



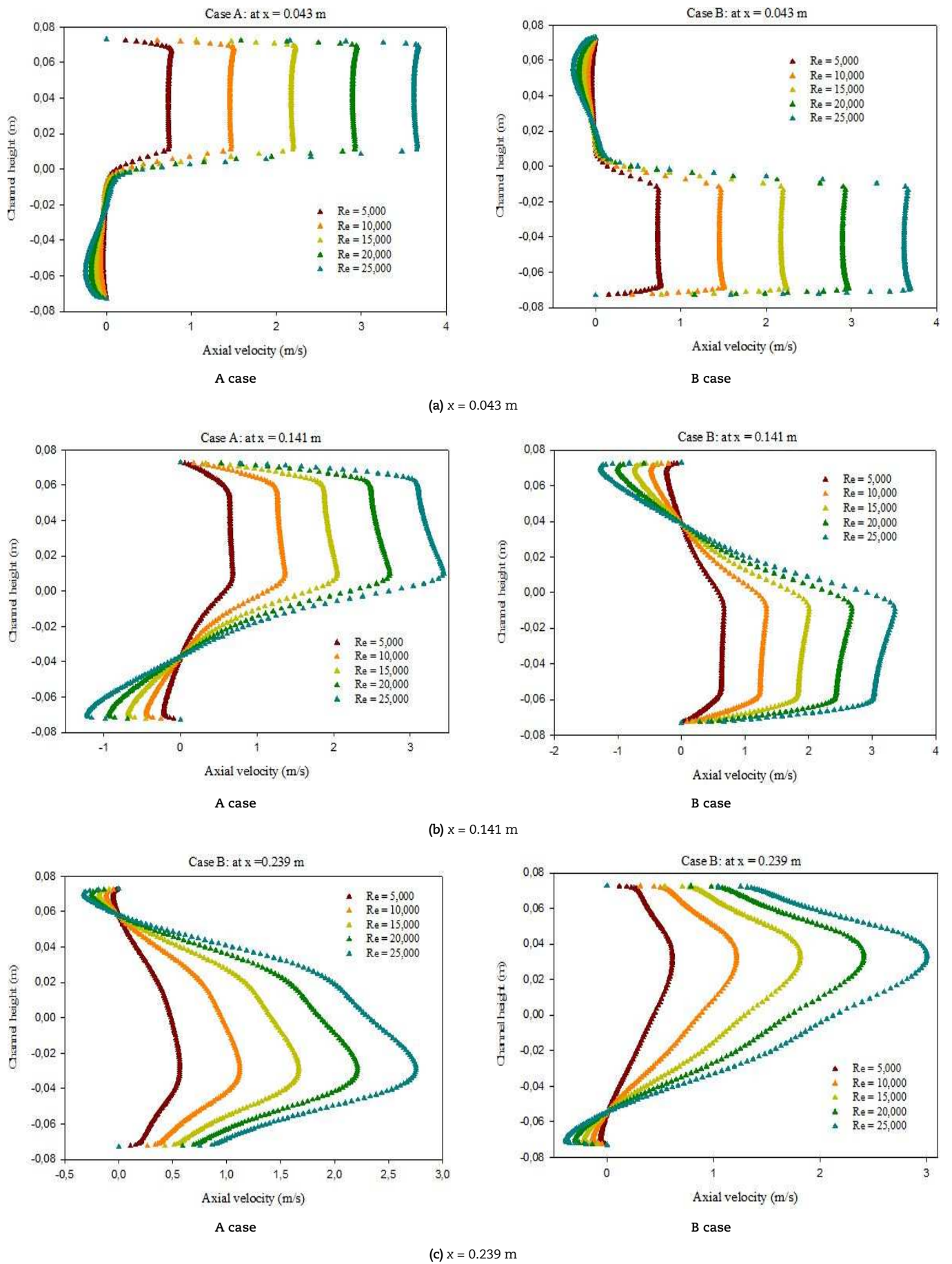


Fig. 14. $u = f(Re)$ in both A and B types and different Xs.



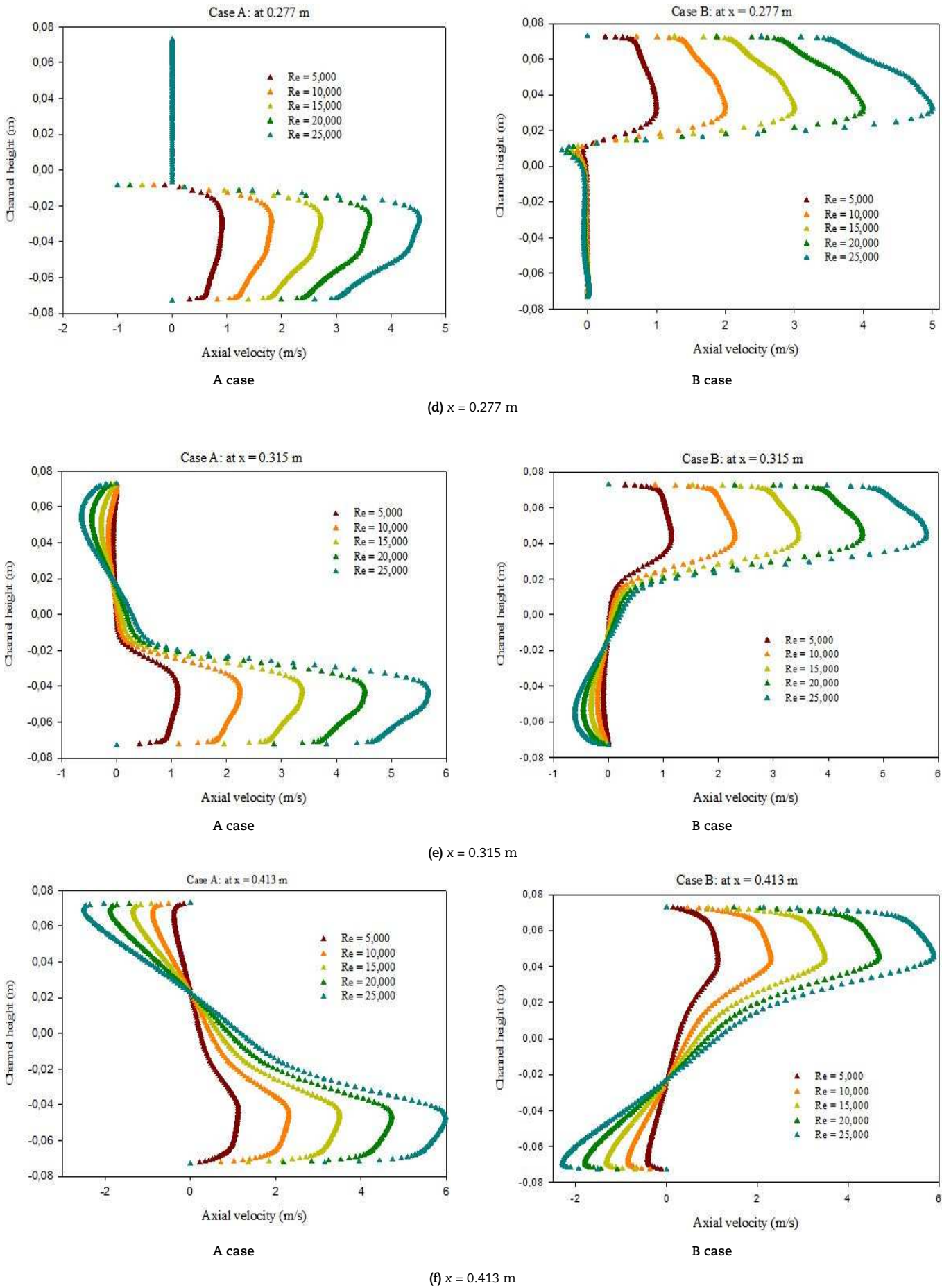


Fig. 14. $u = f(Re)$ in both A and B types and different Xs.



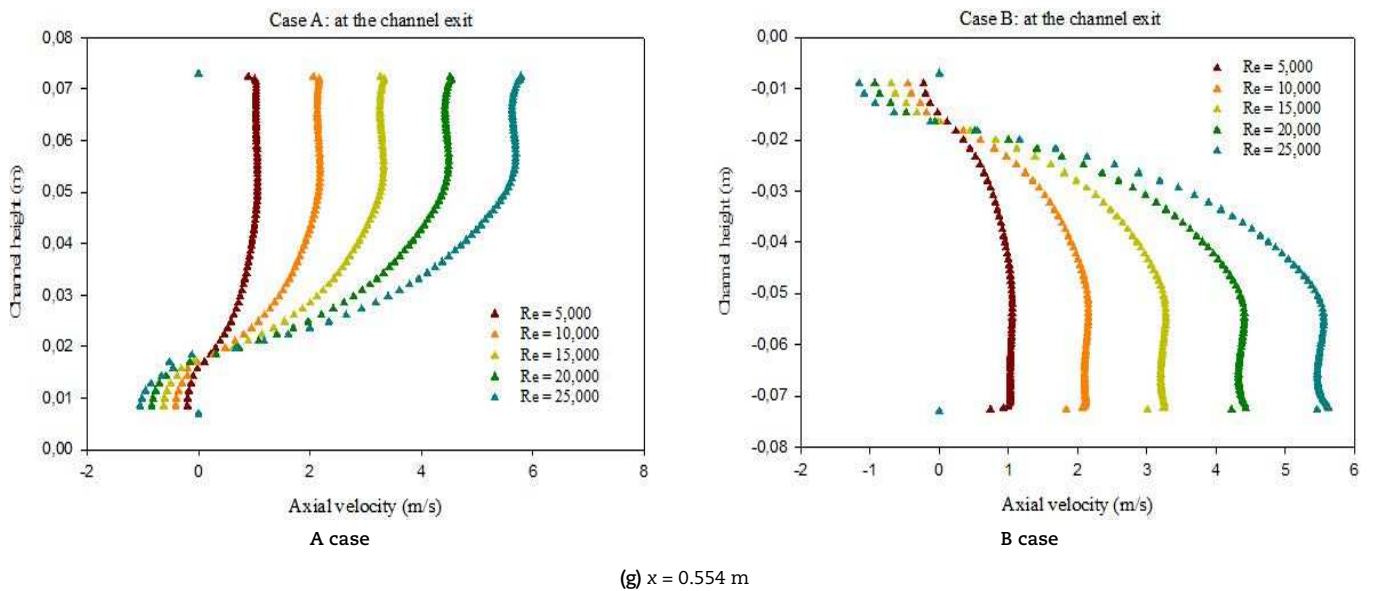


Fig. 14. $u = f(Re)$ in both A and B types and different Xs.

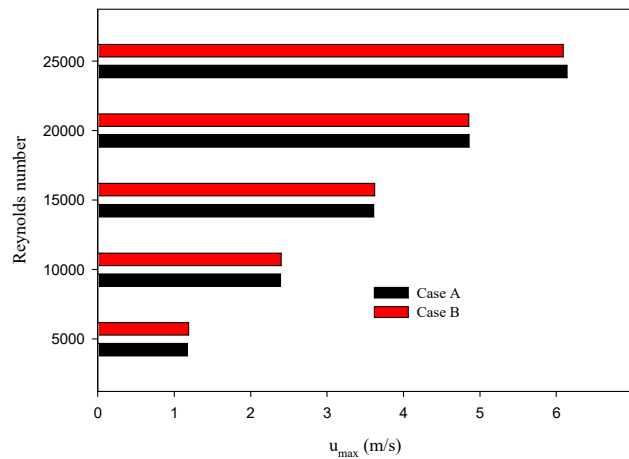


Fig. 15. $u_{max} = f(Re)$ in both A and B models.

- Values of u are very low on the left and right faces of the obstacles due to the low dynamic pressure in these zones. Similar data were reported numerically in [34] and experimentally in [7].
- There is a positive behavior between the u and Re values in both A and B cases. The same observation was also unregistered by [12, 34], for laminar and turbulent regime flows.
- Furthermore, the presence of obstacles inside the first duct (Case A) contributes to the formation of strong cells for recycling with high flow speeds compared to the B second case. This improvement in flow dynamics increases with increasing Re values.

Figs. 6 to 13 show the distribution of X-velocity profiles in both A and B duct models for various axial stations (Xs). The oil current flows from the upper input of the duct in the first case (Case A), while from the lower entrance in the second case (Case B). Starting from the entrance, the velocity profiles are uniform one-dimensional, $u = U_{in}$, on the upper part of the first duct while in the bottom of the second duct (Fig. 6a and b with $x = 0$). The value of u is very poor in the area next to deflector near its right face (Fig. 7a and b with $x = 0.043$ m). These values are negative and indicate a presence of a large vortex of recycling cells as a result of low pressure in this region of the duct (Fig. 8a and b with $x = 0.141$ m). This vortex is a result of the current flow in the mainstream vertical direction. Similar fluid flow phenomenon was found experimentally in [7], and numerically in [34]. The height of this cell of vortex is the same as the height of the obstacle while its extension up to the vicinity of the second obstacle. Besides, u is high between the first-obstacle top-edge and the adjacent duct wall. Next to second-obstacle upper-left-side, small cells for recycling exist. These vortices are the result of the separation of the main flow from the duct wall near this obstacle (Fig. 9a and b with $x = 0.239$ m). While in the opposite region of this same obstacle, the axial velocity values rise due to existing of a small-gap for the stream passage, where the dynamic pressure increases in this region and thus rise in speed values in both cases investigated (Fig. 10a and b with $x = 0.277$ m). As expected, the current is detached on the front upper sharp edge of the second obstacle, leading to the creation of very strong cells for recycling with very low axial velocities on the back region of this same second obstacle (Fig. 11a and b with $x = 0.315$ m). These vortices occupy a large region next to the right face of the second obstacle, which extend up to the gap adjacent to the tip of the last third obstacle (Fig. 12a and b with $x = 0.413$ m). In addition, the current flows at very high velocities, from the top edge of the second obstacle, near the adjacent duct wall, to the upper left side of the last obstacle as well as at the duct exit section (Fig. 13a and b with $x = 0.554$ m).

It is very clear that the values of u are very low for small values of Reynolds number (see Figs. 14 and 15). The u value is enhanced by augmenting Re . This improvement is shown on the back regions of the first and second obstacles (see Fig. 5). This enhancement is due to the presence of recycling cells on their right sides and in both cases.



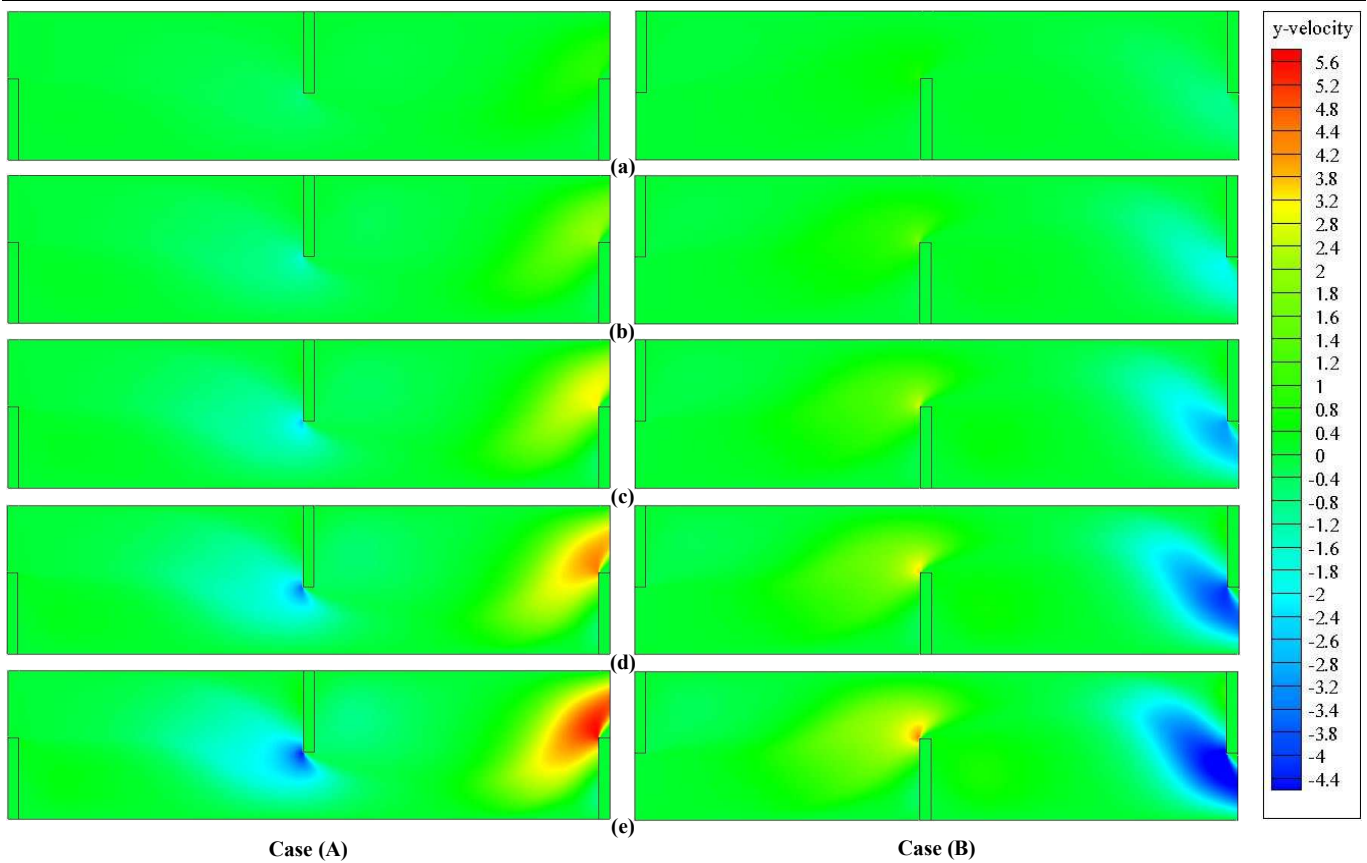


Fig. 16. Contours of Y-velocity in A and B cases: $Re =$ (a) 5×10^3 , (b) 10^4 , (c) 1.5×10^4 , (d) 2×10^4 , (e) 2.5×10^4 .

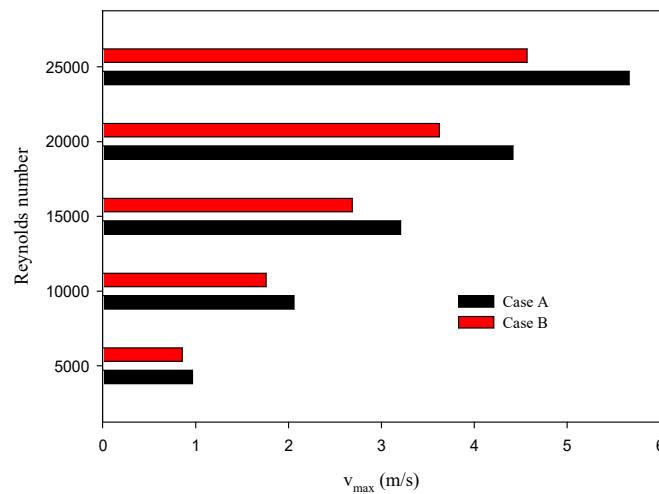


Fig. 17. $v_{max} = f(Re)$ in both A and B models.

In addition, and depending on the two cases studied (A and B), when the Reynolds number is high, the recycling cells are greatly improved in terms of size, length, and strength. The same structure was also reported experimentally by [1] for laminar regime flow, and numerically by [34] for turbulent regime flow. These cells occupy the entire backspace of the obstacles, pushing the current to flow at very high velocities (Fig. 14a-g, with respectively, $x = 0.043$ m, $x = 0.141$ m, $x = 0.239$ m, $x = 0.277$ m, $x = 0.315$ m, $x = 0.413$ m, and $x = 0.554$ m). As expected, the arrangement of obstacles according to the first strategy (Case A) shows an increase in the axial velocity (Fig. 15) with a great support for the recycling cell strength.

The transverse velocity values are very low on the front top sharp edge of the second obstacle, while they are very high on the upper area of the left side of the last third obstacle. This is for the duct case (Case A); unlike the second duct case (Case B). The y-speed change in both direct and reverse directions is increased by raising the Reynolds values in both cases examined, (see Fig. 16 a-e). The first duct (Case A) has better y-velocity values, due to its large recycling cells (see Fig. 17), indicating the advantage of using the baffled and finned duct first model in order to increase the dynamic performance across the smooth ducts, as an enhanced passive method.

5. Conclusion

In this analysis, hydrodynamic field simulations in horizontal rectangular form ducts, using three obstacles with Oil HTF, were reported. Two various finned and baffled duct configurations were treated, i.e., case (A) with one fin and two baffles, and case (B)



with two fins and one baffle. Different oil flow fields, i.e., X-velocity and Y-speed, as well as various X-velocity profiles in many flow stations, related to Re value, were analyzed. A computational approach was applied in order to simulate the Oil flow, basing the Finite Volume (FV) integration method, SIMPLE discretization algorithm, QUICK interpolation scheme, and Standard k-epsilon turbulence model, using ANSYS FLUENT 12.0 software.

- Simulation results reported an unstable flow structure, with powerful recycling cells, on the backsides of each fin and baffle, as a result of fluid detachment on their upper front sharp edges, in both studied models (A and B).
- The u values are very high near the duct walls, between the last two obstacles, as well as near their upper frontal sides. This rise in u is the result of a change in the stream direction due to the turbulators.
- The u values are also increased between the turbulator sharp edges and the duct wall surfaces, due to the higher dynamic pressure values caused by the reduction in the stream surface.
- The u values are very low on the left and right faces of the obstacles due to the low dynamic pressure in these zones.
- There is a direct correlation between the u and Re values in both A and B cases.
- The v velocity values are very low on the front top sharp edge of the second obstacle, while they are very high on the upper area of the left side of the last third obstacle. This is for the duct case (Case A); unlike the second duct case (Case B). The y -speed changes in both direct and reverse directions are increased by raising the Reynolds values in both cases examined.
- Depending on the two cases studied (A and B), when the Re number is high; the recycling cells are greatly improved in terms of size, length, and strength.
- Furthermore, the presence of obstacles inside the first duct (Case A) contributes to the formation of strong cells for recycling with high flow speeds compared to the B second case. This improvement in flow dynamics increases with increasing Re values.
- Finally, the simulation mentioned many physical phenomena such as the turbulence, instability, flow separation, and the appearance of reverse secondary currents. As its data confirmed by many previous numerical and experimental results; the suggested new models of finned and baffled heat exchanger ducts filled with high thermal conductivity oil allow an improvement in the dynamic thermal-energy behavior of many thermal devices such as flat plate solar collectors.
- Many research works in the literature describe the results of experimental research or computer simulations, in which the influence of various types of baffled ducts on the flow dynamics has been studied. This paper confirmed previous observations. The results of this simulation will serve as a database for studying the thermal performance of these solar receptors in future research. This type of analysis is very useful in many industries and engineering-related problems for getting a good idea about the physical model whenever the analytic solution is out of reach.

Author Contributions

Y. Menni numerically simulated the considered physical model; A.J. Chamkha developed the mathematical modeling; and H. Ameer and M.H. Ahmadi analyzed the numerical results. The manuscript was written through the contribution of all authors. All authors discussed the results, reviewed and approved the final version of the manuscript.

Acknowledgments

Not applicable.

Conflict of Interest

The authors declared no potential conflicts of interest with respect to the research, authorship and publication of this article.

Funding

The authors received no financial support for the research, authorship and publication of this article.

Data Availability Statements

The datasets generated and/or analyzed during the current study are available from the corresponding author on reasonable request.

Nomenclature

$C_{1\epsilon}$	Constant used in the standard k- ϵ model	T	Temperature [K]
$C_{2\epsilon}$	Constant used in the standard k- ϵ model	T_{in}	Inlet fluid temperature [K]
$C_{3\epsilon}$	Constant used in the standard k- ϵ model	T_w	Channel wall temperature [K]
C_μ	Constant used in the standard k- ϵ model	S	Source term.
D_h	Aerodynamic diameter of rectangular channel [m]	u	X-velocity of fluid [m/s]
e	Baffle and fin thickness [m]	U_{in}	Inlet fluid velocity [m/s]
f_0	Friction factor for the smooth channel with no fin	v	Y-velocity of fluid [m/s]
h	Baffle and fin height [m]	W	Channel width
H	Channel height [m]	ρ_f	Fluid density [kg/m ³]
k	Turbulent kinetic energy [m ² /s ²]	ρ_s	Solid density [kg/m ³]
L	Channel length [m]	ϵ	Turbulent dissipation rate [m ² /s ³]
L_1	Distance between the first and the second obstacles [m]	Γ	Turbulent diffusion coefficient
L_2	Distance between the second and the third obstacles [m]	μ_e	Effective viscosity [kg/m-s]
P	Pressure [Pa]	μ_l	Laminar viscosity [kg/m-s]
P_{atm}	Atmospheric pressure [Pa]	μ_t	Turbulent viscosity [kg/m-s]
Pr	Prandtl number	τ_w	Wall shear stress [Pa]
Re	Reynolds number	k_f	Fluid thermal conductivity [W/m- C]
S	Source term	k_s	Solid thermal conductivity [W/m- C]



References

- [1] Berner, C., Durst, F., McEligot, D.M., Flow around baffles, *ASME Journal of Heat Transfer*, 106, 1984, 743-749.
- [2] Habib, M.A., Attya, A.E., McEligot, D.M., Calculation of turbulent flow and heat transfer in channels with streamwise-periodic flow, *ASME Journal of Turbomachinery*, 110, 1988, 405-411.
- [3] Yuan, Z.X., Tao, W.Q., Wang, Q.W., Numerical prediction for laminar forced convection heat transfer in parallel-plate channels with streamwise-periodic rod disturbances, *International Journal for Numerical Methods in Fluids*, 28, 1998, 1371-1387.
- [4] Cheng, C.H., Huang, W.H., Numerical prediction for laminar forced convection in parallel-plate channels with transverse fin arrays, *International Journal of Heat Mass Transfer*, 34(11), 1991, 2739-2749.
- [5] Hong, Y.J., Hsieh, S.S., An experimental investigation of heat transfer characteristics for turbulent flow over staggered ribs in a square duct, *Experimental Thermal and Fluid Science*, 4, 1991, 714-722.
- [6] Bazdidi-Tehrani, F., Naderi-Abadi, M., Numerical analysis of laminar heat transfer in entrance region of a horizontal channel with transverse fins, *International Communication in Heat and Mass Transfer*, 31(2), 2004, 211-220.
- [7] Demartini, L.C., Vielmo, H.A., Möller, S.V., Numeric and experimental analysis of the turbulent flow through a channel with baffle plates, *Journal of the Brazilian Society of Mechanical Sciences and Engineering*, 26(2), 2004, 153-159.
- [8] Li, H., Kottke, V., Effect of baffle spacing on pressure drop and local heat transfer in staggered tube arrangement, *International Journal of Heat and Mass Transfer*, 41(10), 1998, 1303-1311.
- [9] Mousavi, S.S., Hooman, K., Heat and fluid flow in entrance region of a channel with staggered baffles, *Energy Conversion and Management*, 47(15), 2006, 2011-2019.
- [10] Pirouz, M.M., Farhadi, M., Sedighi, K., Nemati, H., Fattahi, E., Lattice Boltzmann simulation of conjugate heat transfer in a rectangular channel with wall-mounted obstacles, *Scientia Iranica B*, 18(2), 2011, 213-221.
- [11] Mokhtari, M., Gerdroodbary M.B., Yeganeh, R., Fallah, K., Numerical study of mixed convection heat transfer of various fin arrangements in a horizontal channel, *Engineering Science and Technology*, 20, 2017, 1106-1114.
- [12] Webb, B.W., Ramadhyani, S., Conjugate heat transfer in a channel with staggered ribs, *International Journal of Heat Mass Transfer*, 28, 1985, 1679-1687.
- [13] Wen, J., Yang H., Wang, S., Xue, Y., Tong, X., Experimental investigation on performance comparison for shell-and-tube heat exchangers with different baffles, *International Journal of Heat and Mass Transfer*, 84, 2015, 990-997.
- [14] Dong, C., Zhou, X.F., Dong, R., Zheng, Y.Q., Chen, Y.P., Hu, G.L., Xu, Y.S., Zhang, Z.G., Guo, W.W., An analysis of performance on trisection helical baffles heat exchangers with diverse inclination angles and baffle structures, *Chemical Engineering Research and Design*, 121, 2017, 421-430.
- [15] Skullong, S., Thianpong, C., Jayranaiwachira, N., Promvong, P., Experimental and numerical heat transfer investigation in turbulent square-duct flow through oblique horseshoe baffles, *Chemical Engineering and Processing*, 99, 2016, 58-71.
- [16] Thianpong, C., Yongsiri, K., Nanan, K., Eiamsa-ard, S., Thermal performance evaluation of heat exchangers fitted with twisted-ring turbulators, *International Communications in Heat and Mass Transfer*, 39, 2012, 861-868.
- [17] Nanan, K., Thianpong, C., Pimsarn, M., Chuwattanakul, V., Eiamsa-ard, S., Flow and thermal mechanisms in a heat exchanger tube inserted with twisted cross-baffle turbulators, *Applied Thermal Engineering*, 114, 2017, 130-147.
- [18] Promvong, P., Thermal performance in square-duct heat exchanger with quadruple V-finned twisted tapes, *Applied Thermal Engineering*, 91, 2015, 298-307.
- [19] Eiamsa-ard, S., Wongcharee, K., Eiamsa-ard, P., Thianpong, C., Heat transfer enhancement in a tube using delta-winglet twisted tape inserts, *Applied Thermal Engineering*, 30, 2010, 310-318.
- [20] Chamoli, S., A Taguchi approach for optimization of flow and geometrical parameters in a rectangular channel roughened with V down perforated baffles, *Case Studies in Thermal Engineering*, 5, 2015, 59-69.
- [21] Kumar, R., Kumar, A., Chauhan Ranchan, Sethi Muneesh, Heat transfer enhancement in solar air channel with broken multiple V-type baffle, *Case Studies in Thermal Engineering*, 8, 2016, 187-197.
- [22] Oguntala, G., Abd-Alhameed, R., Haar wavelet collocation method for thermal analysis of porous fin with temperature-dependent thermal conductivity and internal heat generation, *Journal of Applied and Computational Mechanics*, 3(3), 2017, 185-191.
- [23] Davies, T.V., Planetary Atmospheres and Convection in Rotating Fluids, *Nature*, 180(4600), 1957, 1455-1461.
- [24] Sobamowo, G.M., Kamiyo, O.M., Multi-boiling heat transfer analysis of a convective straight fin with temperature-dependent thermal properties and internal heat generation, *Journal of Applied and Computational Mechanics*, 3(4), 2017, 229-239.
- [25] Caccia, M., Tabandeh-Khorshid, M., Itskos, G., Strayer, A. R., Caldwell, A. S., Pidaparti, S., et al., Ceramic-metal composites for heat exchangers in concentrated solar power plants, *Nature*, 562(7727), 2018, 406-409.
- [26] Ghahremani, E., Ghaffari, R., Ghadjar, H., Mokhtari, J., Effect of variable thermal expansion coefficient and nanofluid properties on steady natural convection in an enclosure, *Journal of Applied and Computational Mechanics*, 3(4), 2017, 240-250.
- [27] Amy, C., Budenstein, D., Bagepalli, M., England, D., DeAngelis, F., Wilk, G., et al., Pumping liquid metal at high temperatures up to 1,673 kelvin, *Nature*, 550(7675), 2017, 199-203.
- [28] Akinshilo, A.T., Olofinqua, J.O., Olaye, O., Flow and heat transfer analysis of the sodium alginate conveying copper nanoparticles between two parallel plates, *Journal of Applied and Computational Mechanics*, 3(4), 2017, 258-266.
- [29] Tolstoy, M., Waldhauser, F., Bohnenstiehl, D.R., Weekly, R.T., Kim, W.Y., Seismic identification of along-axis hydrothermal flow on the East Pacific Rise, *Nature*, 451(7175), 2008, 181-184.
- [30] Oguntala, G., Abd-Alhameed, R., Thermal analysis of convective-radiative fin with temperature-dependent thermal conductivity using Chebyshev spectral collocation method, *Journal of Applied and Computational Mechanics*, 4(2), 2018, 87-94.
- [31] Amari, T., Luciani, J.F., Aly, J.J., Small-scale dynamo magnetism as the driver for heating the solar atmosphere, *Nature*, 522(7555), 2015, 188-191.
- [32] Menni, Y., Chamkha, A.J., Lorenzini, G., Ameer, H., Salmi, M., Fridja, D., Numerical simulation of dynamic pressure and kinetic energy fields of turbulent oil flow in staggered baffled pipes, *Mathematical Modelling of Engineering Problems*, 7(1), 2020, 10-16.
- [33] Gholami, M.R., Akbari, O.A., Marzban, A., Toghraie, D., Shabani, G.A.S., Zarringhalam, M., The effect of rib shape on the behavior of laminar flow of oil/MWCNT nanofluid in a rectangular microchannel, *Journal of Thermal Analysis and Calorimetry*, 134(3), 2017, 1611-1628.
- [34] Nasiruddin, Siddiqui, M.H.K., Heat transfer augmentation in a heat exchanger tube using a baffle, *International Journal of Heat and Fluid Flow*, 28, 2007, 318-328.
- [35] Petukhov, B.S., Heat transfer and friction in turbulent pipe flow with variable physical properties, *Advances in Heat Transfer*, 6, 1970, 503-564.
- [36] Launder, B.E., Spalding, D.B., The numerical computation of turbulent flow, *Computer Methods in Applied Mechanics and Engineering*, 3(2), 1974, 269-289.
- [37] Patankar, S.V., Numerical heat transfer and fluid flow, McGraw-Hill, New York, 1980.
- [38] Leonard, B.P., Mokhtari, S., *Ultra-sharp nonoscillatory convection schemes for high-speed steady multidimensional flow*, NASA TM 1-2568, NASA Lewis Research Center, 1990.
- [39] ANSYS Fluent 12.0, Theory Guide, Ansys Inc., 2012.

ORCID iD

Younes Menni  <https://orcid.org/0000-0003-1475-3743>

Ali J. Chamkha  <https://orcid.org/0000-0002-8335-3121>

Houari Ameer  <https://orcid.org/0000-0003-2087-7574>

Mohammad Hossein Ahmadi  <https://orcid.org/0000-0002-0097-2534>



© 2022 Shahid Chamran University of Ahvaz, Ahvaz, Iran. This article is an open access article distributed under the terms and conditions of the Creative Commons Attribution-NonCommercial 4.0 International (CC BY-NC 4.0) license (<http://creativecommons.org/licenses/by-nc/4.0/>).



How to cite this article: Menni Y., Chamkha A.J., Ameer H., Ahmadi M.H. Hydrodynamic Behavior in Solar Oil Heat Exchanger Ducts Fitted with Staggered Baffles and Fins, *J. Appl. Comput. Mech.*, 8(3), 2022, 774–790.
<https://doi.org/10.22055/JACM.2020.32468.2021>

Publisher's Note Shahid Chamran University of Ahvaz remains neutral with regard to jurisdictional claims in published maps and institutional affiliations.

